

ADVANCED ENERGY MATERIALS

Supporting Information

for *Adv. Energy Mater.*, DOI 10.1002/aenm.202500841

Phenothiazine-Based Self-Assembled Monolayer with Thiophene Head Groups Minimizes Buried Interface Losses in Tin Perovskite Solar Cells

Valerio Stacchini, Madineh Rastgoo, Mantas Marčinskas, Chiara Frasca, Kazuki Morita, Lennart Frohloff, Antonella Treglia, Thomas W. Gries, Orestis Karalis, Vytautas Getautis, Florian Ruske, Annamaria Petrozza, Norbert Koch, Hannes Hempel, Tadas Malinauskas, Antonio Abate* and Artem Musiienko**

Supporting Information

For

Phenothiazine-Based Self-Assembled Monolayer with Thiophene Head Groups Minimizes Buried Interface Losses in Tin Perovskite Solar Cells

Authors: Valerio Stacchini^{§ 1,3}, Madineh Rastgoo^{§ 2}, Mantas Marčinskas⁵, Chiara Frasca^{1,3}, Kazuki Morita¹, Lennart Frohloff⁴, Antonella Treglia⁶, Thomas W. Gries, Orestis Karalis¹, Vytautas Getautis⁵, Florian Ruske¹, Annamaria Petrozza⁶, Norbert Koch^{1,4}, Hannes Hempel¹, Tadas Malinauskas^{5*}, Antonio Abate^{1,2,3*}, Artem Musiienko^{7*}

Affiliations:

1. Helmholtz-Zentrum Berlin für Materialien und Energie GmbH, 12489 Berlin, Germany
2. Department of Chemical, Materials and Production Engineering, University of Naples Federico II, Fuorigrotta, Italy
3. Department of Chemistry, University of Bielefeld, [Universitätsstraße 25, 33615 Bielefeld, Germany](#)
4. Institut für Physik & Center for the Science of Materials (CSMB), Humboldt-Universität zu Berlin, 12489, Berlin
5. Department of Organic Chemistry, Kaunas University of Technology, Radvilenu pl. 19, Kaunas LT-50254, Lithuania
6. Istituto Italiano di Tecnologia (IIT), via Rubattino 81, 20134, Milan, Italy
7. Young Investigator Group, Robotized Material and Photovoltaic Engineering, Helmholtz-Zentrum Berlin für Materialien und Energie (HZB), Berlin, Germany.

§ These authors contributed equally to this work

* Corresponding authors: artem.musiienko@helmholtz-berlin.de, antonio.abate@helmholtz-berlin.de, tadas.malinauskas@ktu.lt

Keywords: Self-assembled Monolayers, Buried Interface, Phenothiazine, Tin perovskite, Solar Cells, DMSO-free, Lead-free

Materials and Devices

Chemicals

ITO substrates were purchased from Ossila. Water-free PEDOT complex dispersion in toluene (HTL3) was acquired from Clevios™. Formamidinium iodide was obtained from Dyenamo. Silver shots were supplied by Alfa Aesar and C60 was purchased from CreaPhys. All other chemicals, including SnI₂, Al₂O₃, Ethane-1,2-diammonium iodide, Bathocuproine (BCP), DEF (N,N-diethylformamide), DMPU (N,N'-dimethylpropyleneurea), N,N-dimethylformamide (DMF), toluene, ethanol, and diethyl ether (DEE), were provided by Sigma-Aldrich.

Solar cell preparation

The ITO substrates underwent a sequential cleaning process through sonication, starting with a 2% Hellmanex solution in deionized water, followed by deionized water, acetone, and 2-propanol, each sonicated for 15 minutes. Then, the substrates were subjected to a UV-ozone treatment for 30 minutes and moved into a nitrogen-filled glovebox for further processing. For Th-2EPT dip coating deposition, following the UV-ozone treatment, the substrates were placed in a petri dish containing a SAM solution inside the glovebox (0.2 mM), and the lid was then closed. The substrates were left in the solution for 12 hours. After this period, the substrates were removed, spin-coated at 6000 rpm for 30 seconds, and annealed at 150 °C for 15 minutes. For the spin-coating deposition, a 2 mM stock solution was prepared in DMF. Th-2EPT solution (100 μL) was applied to the pre-cleaned ITO substrates, and after a 10-second delay, the substrates were spin-coated at 6000 rpm for 30 seconds. Subsequently, the SAM-coated substrates were annealed at 150 °C for 15 minutes. For the PEDOT devices, a diluted PEDOT-complex (100 μL, diluted 1:6 v in dry toluene) was dynamically deposited onto the ITO substrates and annealed at 150 °C for 10 minutes. To prepare the absorber layer, stock solutions of SnI₂ (1.2 M) and EDAI₂ (1 M) were prepared in a solvent system consisting of N,N-diethylformamide (DEF) and N,N'-dimethylpropyleneurea (DMPU) in a 1:6 volume ratio. These solutions were left overnight in a shaker at 20 °C. FAI powder was weighed in a vial and mixed with the SnI₂ stock solution in the appropriate amount to reach 1:1.1 FAI:SnI₂ stoichiometry. Finally, the perovskite final solution was prepared by mixing FASnI₃ with 5% EDAI₂. This solution was then spin-coated onto the substrates, first at 500 rpm for 5 seconds and then at 4000 rpm for 40 seconds. At the 22-second, 100 μL of diethyl ether (DEE) was added to the spinning substrate to promote perovskite crystallization. The resulting film was annealed at 100 °C for 30 minutes. The device

fabrication was completed by evaporating layers of C60 (40 nm), BCP (7 nm), and finally a layer of silver (140 nm).

Methods

Density Functional Theory (DFT) Calculations

The all-electron numeric-atom-centred orbital code FHI-aims was used to carry out the DFT calculations¹. The molecular structure of MeO-2PACz and Th-2EPT was determined by performing DFT structure optimization with B3LYP exchange-correlation functional². For FASnI₃, α -phase FASnI₃ was relaxed with reciprocal space sampling of $5 \times 5 \times 5$. The molecular calculation and the bulk calculation were performed with open and periodic boundary conditions, respectively. The relaxed bulk FASnI₃ was then used to construct a SnI₂ terminated (001) surface slab model with an area of 4×3 -unit cells and four layers in thickness. With periodic boundary conditions, the bottom two layers were fixed, and the rest was allowed to relax. From the observation that the anchoring group is bound to ITO and does not fold back as in the stable conformers, we replaced the anchoring group beyond phosphorus with hydrogen. The SAM on the surface were modelled by placing MeO-2PACz and Th-2EPT so that oxygen and sulfur were over the surface I-site, respectively. Since the distance between the chalcogens did not exactly match the I-I distance, we calculated two different bonding configurations each (Figure S1). During the relaxation, both SAM and surface were allowed to relax, and the calculation was performed with reciprocal space sampling of $1 \times 1 \times 1$ and B3LYP functional. For the calculation of binding energy, we closely followed the definition: the energy required to remove the molecule from the surface. We therefore calculated the energy difference between the SAM binded to the surface and when they are isolated.. To check the effect of dipole within the calculation cell, we performed the same calculation with dipole correction and confirmed that the effect of dipole is negligible. Furthermore, basis set superposition error (BSSE) for B3LYP

is smaller than in post-Hartree-Fock methods (e.g. Møller–Plesset methods)³, therefore BSSE correction was omitted.

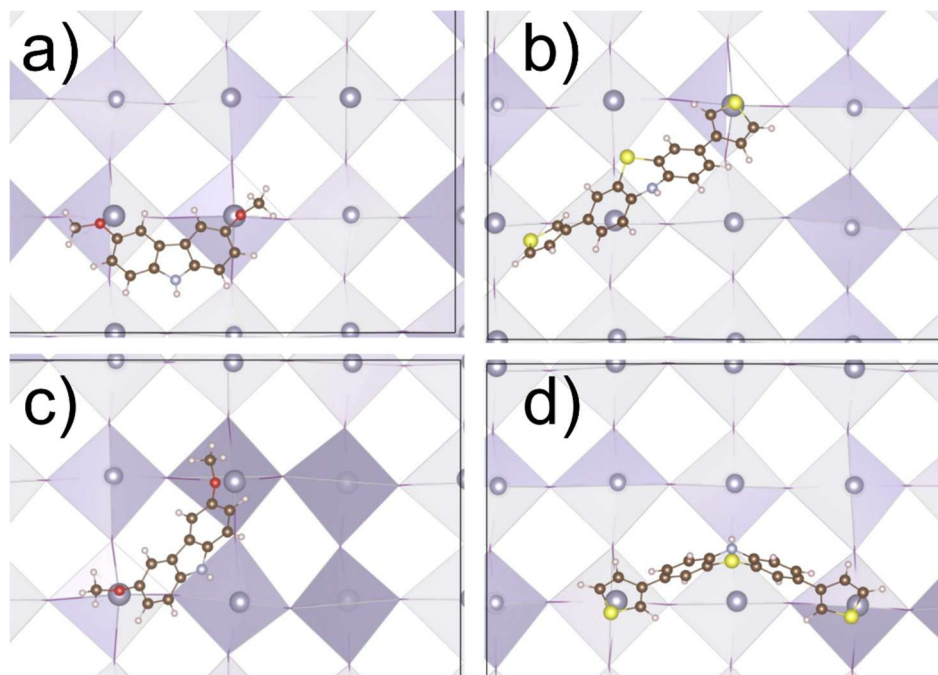


Figure S1 DFT optimized molecular structure of MeO-2PACz **(a)** and **(c)**, and Th-2EPT **(b)** and **(d)** on FASnI₃ surface.

Lattice Matching of SAMs

To assess the geometric compatibility between the SAM molecules and the FASnI₃ surface ($a \approx 6.3$ Å for FASnI₃), we evaluated the lateral distance between their passivating atoms (O–O in MeO-2PACz and S–S in Th-2EPT) and compared these with projected interatomic spacings of Sn atoms at the SnI₂-terminated (100) surface of cubic FASnI₃. The α -phase of FASnI₃ adopts a pseudo-cubic perovskite structure (space group $Pm\bar{3}m$), where tin atoms occupy the corner positions of a simple cubic lattice. Starting from a reference Sn atom at (0,0,0), the positions of its neighbors can be defined by integer lattice vector displacements in 3D space, and the interatomic distances can be calculated using the Euclidean norm. For example, the first-nearest neighbors lie at positions like (a,0,0), (0,a,0), (0,0,a), with a distance of a , the cubic lattice constant. Higher-order neighbors are located along face diagonals (e.g., $\sqrt{2}a$), body diagonals ($\sqrt{3}a$), and further out. We computed the Sn–Sn distances up to

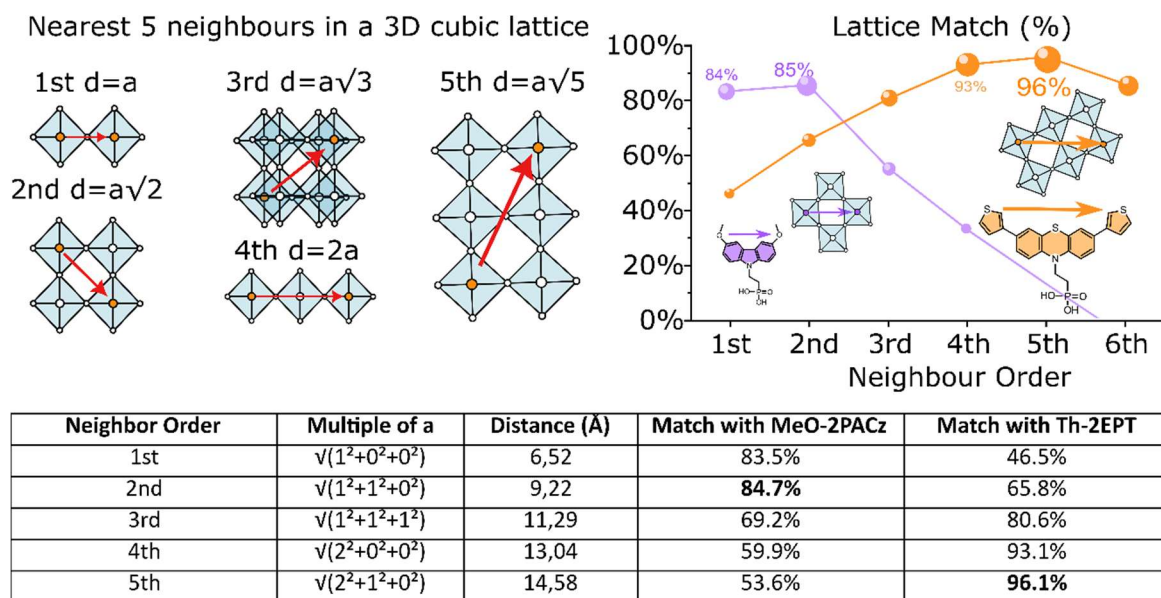


Figure S2 Lattice match calculations. In the upper left figure, a graphical representation of lattice vectors corresponding to the first 5 nearest neighbouring Sn ions in the FASnI_3 cubic tridiemnsional lattice. On the right, a plot represents Lattice match as a function of the neighbouring order. Below, the same data is reported in a table.

the fifth-nearest neighbors using this approach and projected these vectors onto the (100) surface to simulate the surface lattice viewed from above. The O–O distance in MeO-2PACz is approximately 7.81 Å, which best aligns with the second-nearest Sn–Sn spacing of ~9.22 Å, resulting in a geometric match of ~85%. In contrast, Th-2EPT has a head group S–S spacing of ~14.01 Å, which aligns closely with the fifth-nearest Sn–Sn distance (~14.6 Å), achieving a 96% match. The better geometric compatibility of Th-2EPT with the natural periodicity of the surface suggests reduced interfacial strain and improved lattice templating. A full table of calculated Sn–Sn spacings, neighbor indices, and match percentages is provided in Figure S2, along with a visual representation of neighbor shells in the 3D perovskite lattice.

X-Ray Diffraction (XRD)

XRD was carried out on a Bruker D8 diffractometer in Bragg–Brentano geometry, using $\text{Cu K}\alpha$ radiation ($\lambda = 1.5406 \text{ \AA}$), 40 kV acceleration voltage, and 40 mA current. Samples were measured under inert conditions using airtight poly(methyl methacrylate) (PMMA) sample holders by Bruker. To remove background noise and any sloping baseline, an asymmetric least squares (ALS) algorithm was applied to each dataset. To aid in peak visual clarity and detection, a mild smoothing filter was applied to the baseline-corrected data. A simple moving average (window ~11 points, corresponding to ~0.22°) was used to reduce high-frequency noise. All peak-finding operations were performed on these smoothed intensity curves. (Notably, smoothing was only used for identifying and plotting peaks; the quantitative peak fitting for obtaining FWHM employed the original unsmoothed data to

preserve accuracy). An automated peak-finding algorithm (SciPy's `find_peaks`) scanned each smoothed XRD pattern to identify significant diffraction peaks. A Gaussian fit of the (100) peak for each sample yielded the peak position (around $14.3^\circ 2\theta$) and the **FWHM** (full width at half maximum) in degrees. The table below summarizes the measured peak position and FWHM for the (100) reflection of each sample. All three samples have essentially the same peak position within $\sim 0.1^\circ$, but their FWHM values differ significantly.

Sample	(100) Peak Position ($^\circ 2\theta$)	FWHM ($^\circ 2\theta$)
PEDOT	14.38 $^\circ$	0.10 $^\circ$
MeO	14.30 $^\circ$	0.30 $^\circ$
Th-2EPT	14.30 $^\circ$	0.12 $^\circ$

Scanning Electron Microscope (SEM) Imaging

SEM images were collected using a Zeiss Merlin SEM with a Gemini 2 column. Samples were transferred from the glovebox to the SEM inside an airtight transfer shuttle in inert ambient. Images from the top (figure 2) were collected with an acceleration voltage of 2 kV and recorded with an Everhart-Thornley detector to highlight the topological contrast.

UV-Vis Absorbance Spectra and Photoluminescence Quantum Yield (PLQY)

UV-vis steady state spectra were measured on perovskite thin films deposited on bare glass using a UV/VIS/NIR spectrophotometer Lambda 1050, PerkinElmer, in the wavelength range 350–1100 nm, a step size of 1 nm. The excitation density dependent PLQY measurement was performed by illuminating the sample from the glass side with a femtosecond laser (Light conversion Pharos) at 500 kHz and wavelength of 343 nm and with variable power density. The photoluminescence was collected in reflection geometry with a Maya 2000 Pro visible spectrometer.

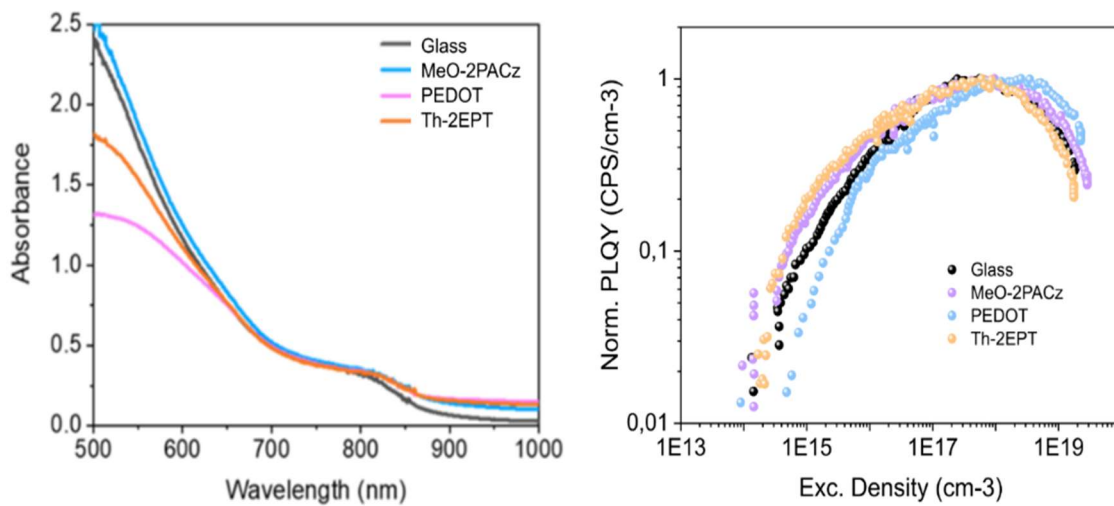


Figure S3 Absorbance spectra (UV-vis) of thin films of tin perovskite coated on top the different HTL substrates. Normalized PLQY obtained from the same samples.

Transient Absorption Spectroscopy (TA)

For TAS characterization an amplified femtosecond laser (Light Conversion Pharos) generated pulses of ~ 280 fs centred at 1030 nm with a repetition rate of 2 kHz. A broadband white light probe is generated by focusing the pulses into a thin sapphire plate. At short delays (< 5 ns), the third harmonic of the fundamental provided the pump light (343 nm). At long delays (> 1 ns), pump light at 354 nm was provided by the second harmonic of a Q-switched Nd:Yag laser (Innolas Picolo), which was electronically triggered and synchronized to the femtosecond laser via an electronic delay. The pump excitation density is $4 \cdot 10^{17} \text{ cm}^{-3}$.

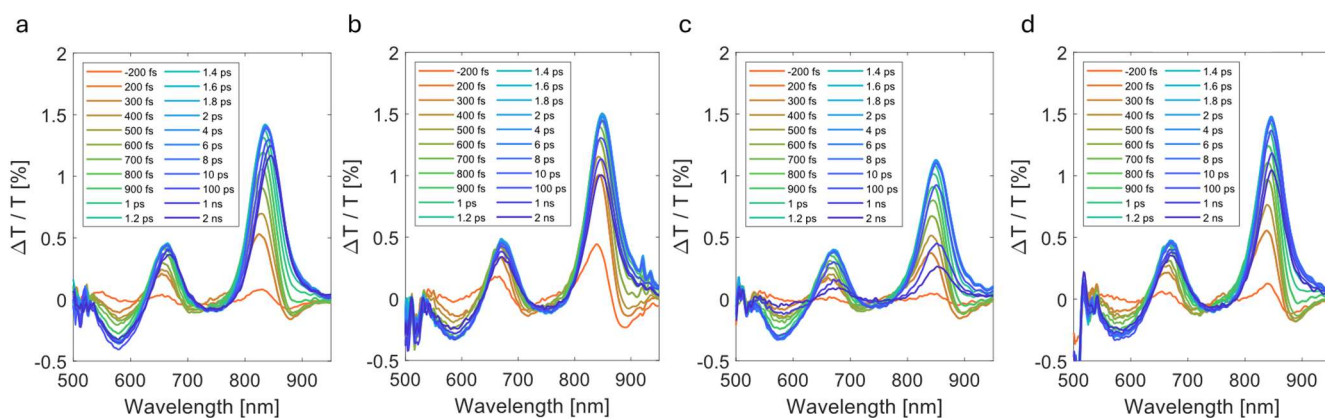


Figure S4 Transient Absorption Spectra of perovskite on a) glass, b) MeO-2PACz, c) PEDOT, d) Th-2EPT as function of pump-probe delay

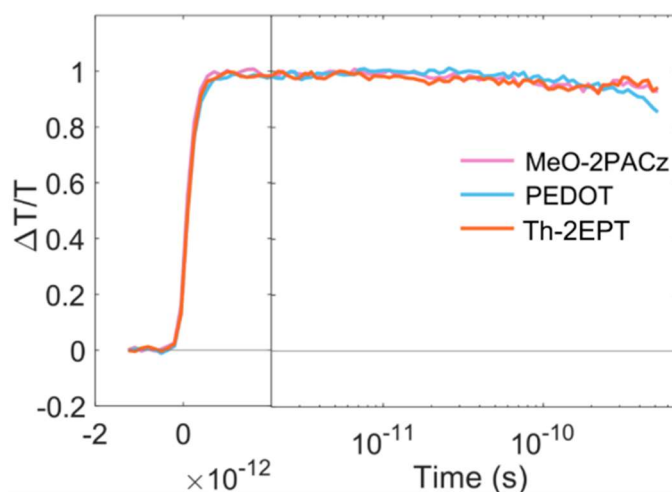
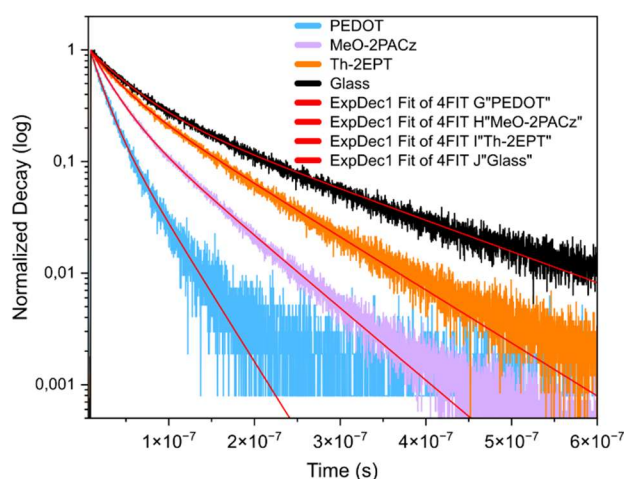


Figure S5 Transient Absorption Spectra of perovskite on a) glass, b) MeO-2PACz, c) PEDOT, d) Th-2EPT as function of pump-probe delay

Transient Photoluminescence (trPL)

Tr-PL is a common technique for measuring charge carrier recombination in semiconductors. The samples were excited with a femtosecond laser of 515 nm wavelength and repetition rate of 125 kHz. The laser power was attenuated with neutral density filters to $2.4 \text{ pJ} \cdot \text{cm}^{-2}/\text{pulse}$. This corresponds to a photoexcitation of $6 \cdot 10^{13} \text{ carriers} \cdot \text{cm}^{-3}$. This carrier concentration is typical for such perovskite thin films to open circuit conditions under 1 sun illumination. The PL emission was measured by time-correlated single photon counting with PicoHarp300. To this end, a Geiger-mode avalanche photodiode was used with a 530 nm long-pass filter in front of it to suppress the 515 nm laser light.



	A1		t1		A2		t2		Statistics	
		Standard Error		Standard Error		Standard Error		Standard Error	Reduced Chi-Sqr	Adj. R-Square
PEDOT	1,1488	0,0053	1,39322E-8	7,32077E-11	0,45645	0,00682	3,53863E-8	1,97917E-10	4,93572E-6	0,99545
MeO-2PACz	0,91409	0,00176	2,31897E-8	5,27698E-11	0,42742	0,00214	6,70477E-8	1,48326E-10	2,5283E-6	0,99876
Th-2EPT	0,6101	0,00162	3,0238E-8	9,42536E-11	0,56078	0,00192	9,14255E-8	1,455E-10	3,7762E-6	0,99874
Glass	0,74573	0,00113	4,24039E-8	9,37459E-11	0,38858	0,00133	1,55602E-7	2,94338E-10	7,87264E-6	0,99795

Figure S6 Double exponential fitting parameters derived from the time-resolved photoluminescence (trPL) measurements. The plots display the raw trPL data with the corresponding fitted curves overlaid for comparison.

Solar Cells

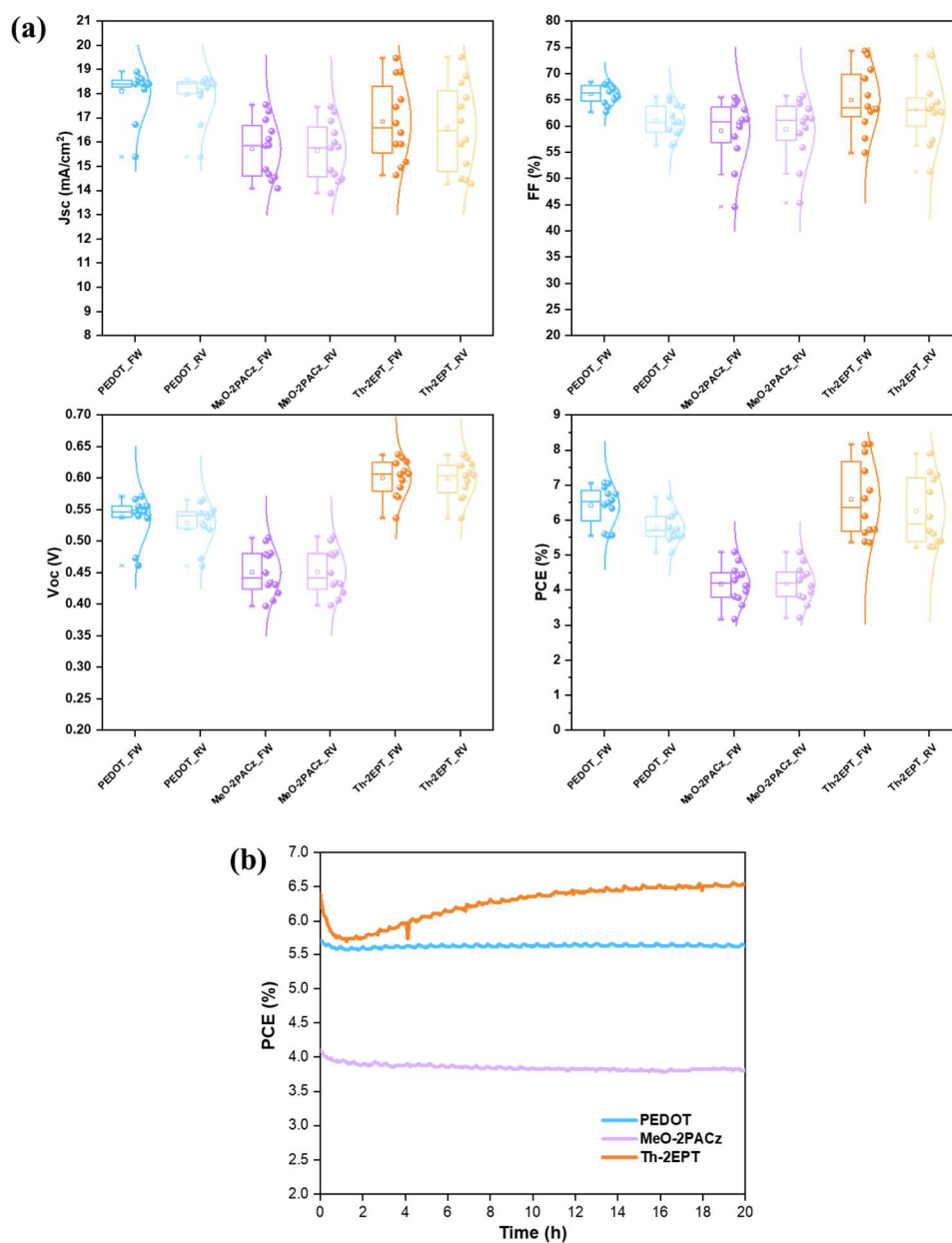


Figure S7 (a) J_{sc} , FF, V_{oc} , and PCE statistics from both forward and reverse JV scans of tin perovskite solar cells (TPSCs). (b) Short-term operational stability of TPSC devices under continuous one-sun illumination in a nitrogen atmosphere.

We compared the operational stability of devices with different HSLs under maximum power point (MPP) tracking in a nitrogen atmosphere. The devices based on PEDOT and MeO-2PACz showed similarly stable performance over 20 hours. In contrast, the Th-2EPT device initially exhibited a decline in performance during the first 2 hours, followed by a noticeable recovery as the test progressed.

Contact Angle Measurement

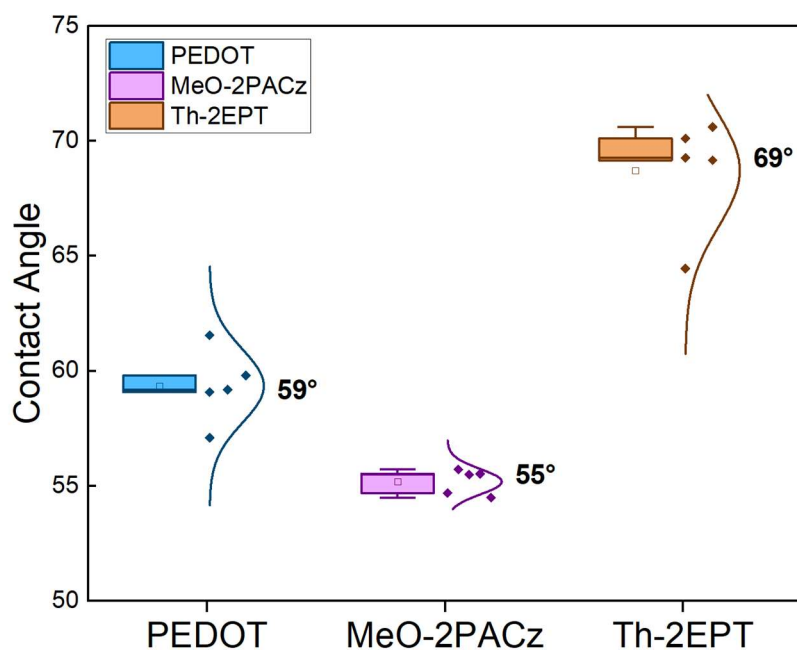


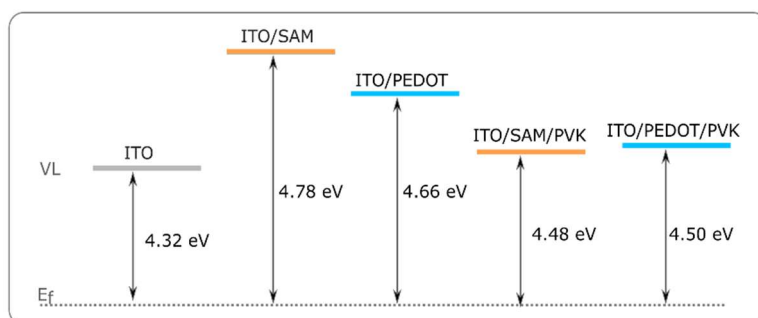
Figure S8 Contact angle measurements for PEDOT, MeO-2PACz, and Th-2EPT layers deposited on ITO substrates. Th-2EPT exhibits a contact angle of 69°. PEDOT achieves a contact angle of 59°, aided by an alumina nanoparticle interlayer. MeO-2PACz displays the lowest contact angle (55°).

Ultraviolet Photoemission Spectra (UPS) and X-ray Photoemission Spectra (XPS)

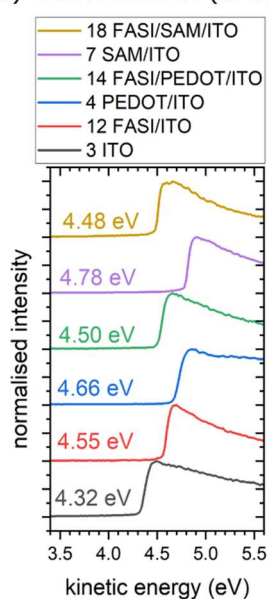
The ultraviolet photoemission spectra were recorded using a hemispherical electron analyser (SPECS Phoibos 100) in a UHV system equipped with a monochromated He I ($h\nu = 21.218$ eV) source. The selected pass energy 5 eV offers a setup resolution of 105 meV as determined from the Fermi edge of sputter-annealed gold. The base pressure of the analysis chamber was 3×10^{-10} mbar. All spectra were recorded under normal emission with an acceptance angle of ca. 6° . For measurement of the SECO, a sample bias of -10.0 V was employed to overcome the analyser work function. The low-energy inverse photoemission spectra were recorded using a LEIPES system (ADCAP Ltd.) consisting of an electron gun with a BaO cathode and a Hitachi photomultiplier tube behind a 250 ± 6 nm bandpass filter in a UHV chamber with base pressure better than 1×10^{-9} mbar. The setup resolution was determined to be 600 meV. The x-ray photoemission spectra were acquired with a JEOL JPS-9030 with a vacuum base pressure of 3×10^{-9} mbar using monochromated Al $K\alpha$ radiation ($h\nu = 1486.6$ eV) for excitation. The spectra were recorded with pass energy 20 eV, resulting in a setup resolution of 820 meV as determined from the FWHM of the Ag 3d_{5/2} peak and under an emission angle of $\sim 10^\circ$. All spectra were recorded at room temperature. In order to establish the energy level alignment at the FASI/Th-2EPT and FASI/PEDOT interfaces, photoemission spectroscopy measurements were performed. The samples were prepared ex-situ in a nitrogen-filled glovebox and transferred into the UHV system without air exposure. All measurements were performed within three days after sample fabrication.

UPS characterisation

a) Energy level diagram from UPS and KP data



b) Work Function (UPS)



c) Work function (Kelvin Probe)

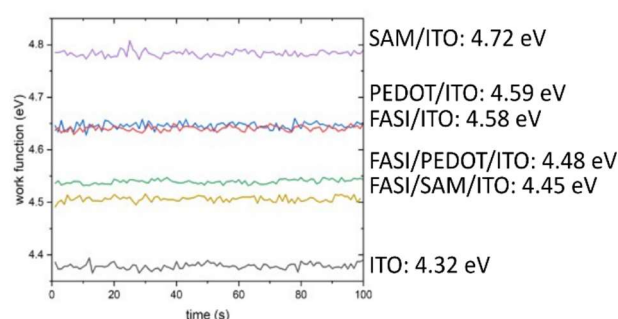


Figure S9 energy level diagram (a) obtained from UPS Measurements for kinetic and binding energy (b) and Kelvin Probe for work function values (c).

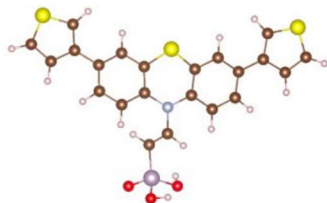
In Figure S9 the secondary electron cut-offs of the ITO substrate, HTL/ITO and FASI/HTL/ITO are shown for PEDOT and Th-2EPT SAM. The work function of the ITO substrate was determined to be 4.32 eV and slightly increases to 4.78 eV and 4.66 eV after deposition of the SAM or PEDOT, respectively. The increase of the work function upon deposition of the SAM can be rationalised by means of the dipole character of the Th-2EPT SAM⁴. The electron attracting nature of the thiophene groups causes a molecular dipole pointing away from the sample surface and thereby provides an additional barrier for electron emission, consequently slightly increasing the work function. This effect can be quantified by the means of the Helmholtz equation:

$$\Delta\Phi = \frac{e\mu_{\perp} N}{\epsilon_0\epsilon_r A} = \frac{e\mu \cos \theta N}{\epsilon_0\epsilon_r A}$$

The stronger the dipole moment of the molecule and the higher the molecule density per area, the higher the work function change upon SAM deposition. [Inserting $\Delta\Phi = 0.46$ eV, assuming a dipole moment of $\mu = 0.61$ eÅ as calculated from DFT and a dielectric constant $\epsilon_r = 2$,⁴ that gives the tilt angle of the molecule θ and the molecule density per area N/A as unknown parameters. For hypothetical tilt angle of 0° (perpendicular to surface) this gives $N/A = 0.83$ nm⁻². Calculating for other angles: $\theta = 30^\circ$ gives $N/A = 0.96$ nm⁻², $\theta = 45^\circ$ gives $N/A = 1.18$ nm⁻². For comparison: 1 nm⁻² is approximately one molecule per ITO unit cell⁵. After deposition of FASI, all samples show a work function around 4.50 eV. The independence of the FASI energy levels concerning the substrate work function points to pinning of the Fermi level. The strong p-type character matches up with the well-known self-doping in tin perovskites.⁶ The slight positive barrier for hole extraction should, however, not limit the functionality of the solar cell as the SAM layer is only less than one nanometre thin. All work functions measured through UPS were further confirmed with vacuum Kelvin Probe measurements to exclude any influence by the high-energy radiation required for UPS. Further, no surface photo voltage greater than 50 meV was detected for any sample at additional 1.5 suns white light illumination during UPS measurements. In Fig. S9, a schematic representation of the energy level alignments in the respective half-cells is depicted. For FASI, a negligible exciton binding energy is assumed as rationalised for other perovskites.

XPS characterisation

a) molecular structure of Th-2EPT



b) peak areas for different XPS signals

Orbital	Area	RSF	Area/RSF
S 2p	62	1.54	40.3
P 2p	16	1.11	14.4
N 1s	24	1.73	13.9
C 1s	328	1.00	328
In 3d	5473	10.90	502.1

c) Phosphorous, sulfur, nitrogen specific peaks

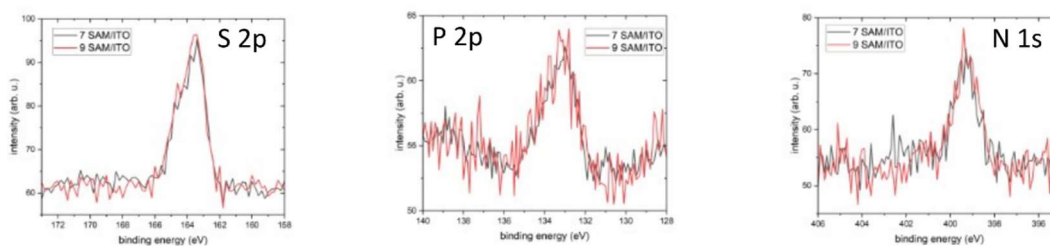


Figure S10 XPS Spectra showing a model of the molecular structure from the software Avogadro; **b)** peak areas ratios for different elemental orbitals [RSF = Relative Sensitivity Factor]; **c)** specific peaks.

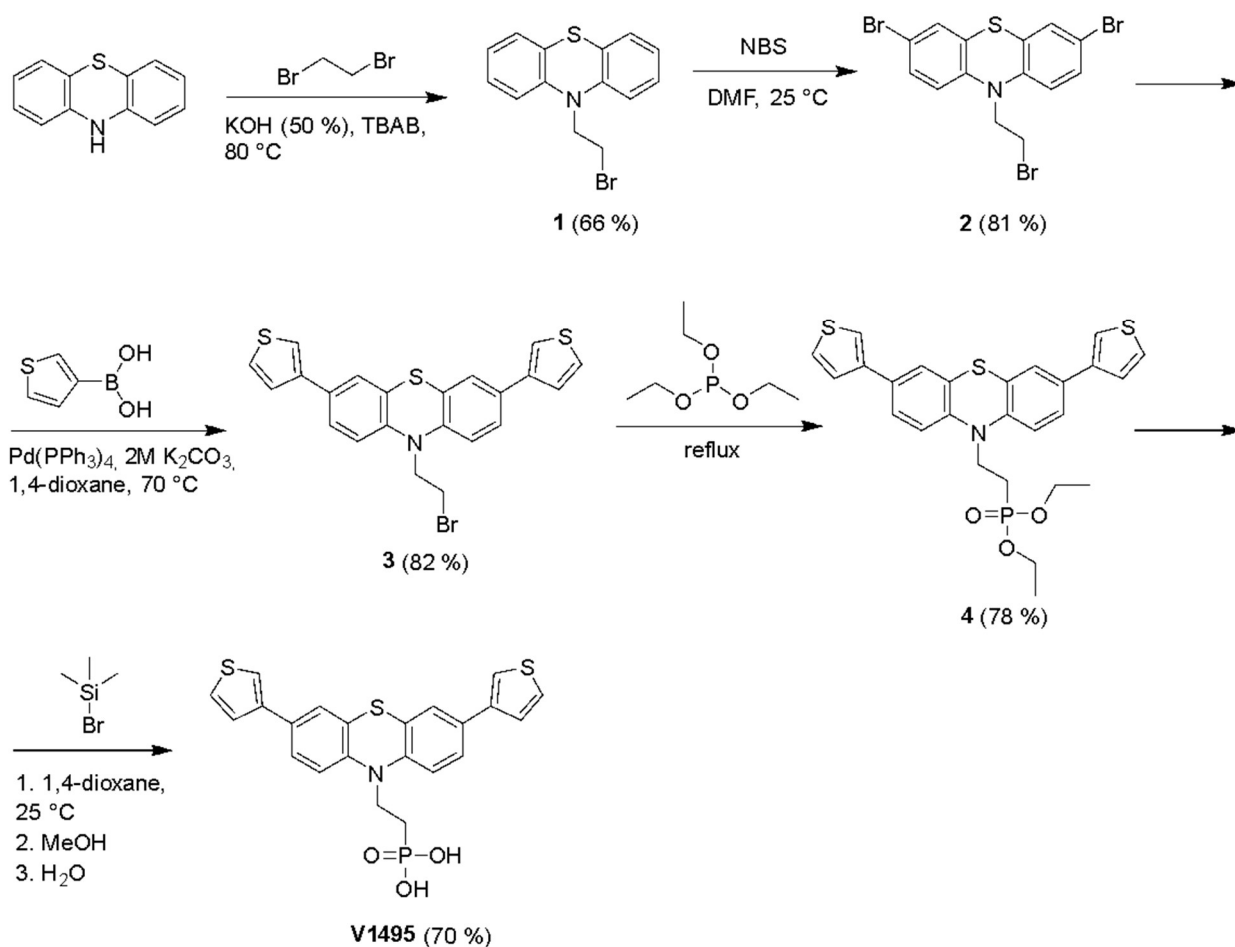
The x-ray photoemission spectroscopy confirms the presence of the Th-2EPT molecule on the ITO surface. A quantitative analysis of the SAM/ITO data confirms the expected stoichiometry between P:S:N:C within the molecule to be 1.0:2.8:1.0:23 (expected: 1:3:1:22). The density of SAM binding could not be extracted from the measurement, but the presence of the molecule on ITO is confirmed.

Synthesis of Th-2EPT (V1495)

Chemicals were purchased from Sigma-Aldrich, TCI Europe, and used as received without further purification. ^1H NMR spectra were recorded at 400 MHz on a Bruker Avance III spectrometer, ^{13}C NMR spectra were collected using the same instrument at 101 MHz. The chemical shifts, expressed in ppm, are reported relative to tetramethylsilane (TMS). Reactions were monitored by thin-layer chromatography on ALUGRAM SIL G/UV254 plates and developed with UV light. Silica gel (grade 9385, 230–400 mesh, 60 Å, Aldrich) was used for column chromatography. Elemental analysis was performed with an Exeter Analytical CE-440 elemental analyzer, Model 440 C/H/N/. Electrothermal A.KRÜSS M3000 capillary melting point apparatus was used for determination of melting points.

Synthesis scheme

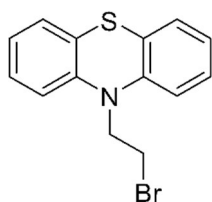
10-*H*-Phenothiazine was alkylated using 1,2-dibromoethane. Alkylated derivative **1** was brominated using *N*-bromosuccinimide in DMF. Isolated phenothiazine **2** was used for the palladium catalyzed Suzuki-Miyaura coupling reaction with 3-thienylboronic acid under argon in anhydrous 1,4-dioxane, resulting in intermediate **3**, which was further transformed into phosphonate **4** by refluxing in triethyl phosphite. Final product Th-2EPT SAM molecule, containing phosphonic acid functional group, was obtained by hydrolysis of obtained intermediate, using bromotrimethylsilane, methanol and water.



Scheme S1. Synthesis route to the phenothiazine-based Th-2EPT SAM (or V1495) containing thiophenes and phosphonic acid anchoring group.

Experimental procedure

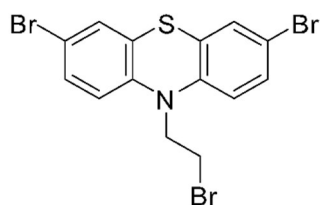
10-(2-bromoethyl)-10H-phenothiazine (**1**)



10H-Phenothiazine (5 g, 25.1 mmol) was dissolved in 1,2-dibromoethane (54 ml, 627 mmol), followed by addition of 50 % KOH aqueous solution (14 ml, 125 mmol) and tetrabutylammonium bromide (1.21 g, 3.76 mmol). Reaction mixture was heated to 80 °C and conducted for 96 hours. After first 24 hours additional 50 % KOH aqueous solution (14 ml, 125 mmol) and tetrabutylammonium bromide (1.21 g, 3.76 mmol) were added. After termination of reaction (TLC, eluent acetone:*n*-hexane, 3:22), organic components were extracted with ethyl acetate, organic layer

dried over anhydrous Na₂SO₄, filtered and solvent removed under reduced pressure. Crude product was purified by column chromatography (eluent acetone:*n*-hexane, 3:22). Product obtained as yellow crystals (5.12 g, 66 % yield). M.p. 78–80 °C. ¹H NMR (400 MHz, DMSO-*d*₆): δ 7.24 – 7.13 (m, 4H), 7.04 (d, *J* = 8.1 Hz, 2H), 6.97 (t, *J* = 7.4 Hz, 2H), 4.30 (t, *J* = 6.3 Hz, 2H), 3.74 (t, *J* = 6.3 Hz, 2H) ppm. ¹³C NMR (101 MHz, DMSO-*d*₆): δ 143.96, 127.71, 127.26, 123.99, 122.91, 115.76, 48.36, 29.78 ppm. Anal. calcd. for C₁₄H₁₂BrNS: C 54.91, H, 3.95, N, 4.57; found: C 55.07, H 3.85, N 4.42.

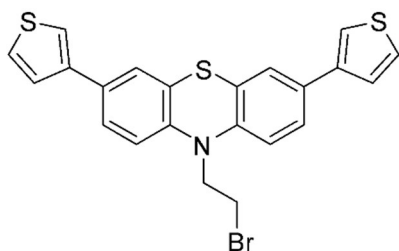
3,7-Dibromo-10-(2-bromoethyl)-10H-phenothiazine (2)



10-(2-Bromoethyl)-10*H*-phenothiazine (**1**, 2 g, 6.53 mmol) was dissolved in DMF (25 ml) and afterwards *N*-bromosuccinimide (2.38 g, 13.4 mmol) was added portionwise. Reaction conducted overnight at 25 °C. After termination of reaction (TLC, eluent acetone:*n*-hexane, 1:24) organic components extracted with ethyl acetate, organic layer dried over anhydrous Na₂SO₄, filtered and solvent evaporated under reduced pressure. Crude product was purified by column chromatography (eluent acetone:*n*-hexane, 1:24), resulting in white crystals (2.44 g, 81 % yield) as a product. M.p. 144–145 °C.

¹H NMR (400 MHz, DMSO-*d*₆): δ 7.39 – 7.32 (m, 4H), 6.98 (d, *J* = 8.6 Hz, 2H), 4.26 (t, *J* = 6.2 Hz, 2H), 3.70 (t, *J* = 6.1 Hz, 2H) ppm. ¹³C NMR (101 MHz, DMSO-*d*₆): δ 143.05, 130.43, 129.21, 125.96, 117.70, 114.52, 48.49, 29.58 ppm. Anal. calcd. for C₁₄H₁₀Br₃NS: C 36.24, H, 2.17, N, 3.02; found: C 36.50, H 2.02, N 2.88.

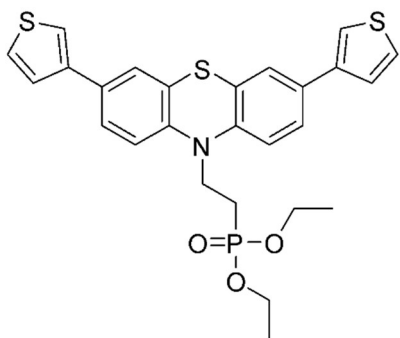
10-(2-Bromoethyl)-3,7-di(thiophen-3-yl)-10H-phenothiazine (3)



3,7-Dibromo-10-(2-bromoethyl)-10*H*-phenothiazine (**2**, 1.5 g, 3.23 mmol) was dissolved in anhydrous 1,4-dioxane (40 ml) under argon atmosphere, followed by addition of 3-thienylboronic

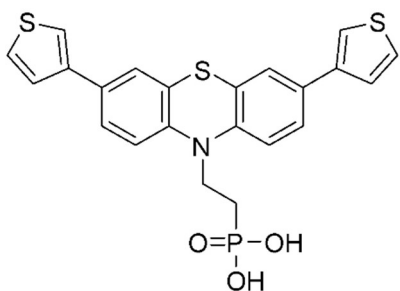
acid (1.03 g, 8.08 mmol), Pd(PPh₃)₄ (0.37 g, 0.32 mmol) and K₂CO₃ 2M aqueous solution (5.9 ml, 9.69 mmol). Reaction conducted at 80 °C under inert argon atmosphere for 24 hours. After termination of reaction (TLC, eluent acetone:*n*-hexane, 2:23), reaction mixture was cooled down and filtered through celite which was washed with THF. Organic solvent was evaporated, and the crude product was purified by column chromatography using acetone:*n*-hexane (2:23) as an eluent resulting yellow crystals (1.24 g, 82 %) as a product. M.p. 177.5–179 °C (melting and decomposition). ¹H NMR (400 MHz, DMSO-*d*₆): δ 7.82 (d, *J* = 1.1 Hz, 2H), 7.62 – 7.58 (m, 2H), 7.57 – 7.48 (m, 6H), 7.10 – 7.01 (m, 2H), 4.35 (t, *J* = 6.1 Hz, 2H), 3.81 – 3.73 (m, 2H) ppm. ¹³C NMR (101 MHz, DMSO-*d*₆): δ 142.55, 140.20, 130.20, 127.03, 126.00, 125.44, 124.65, 124.06, 120.12, 115.95, 48.46, 29.86 ppm. Anal. calcd. for C₂₂H₁₆BrNS₃: C 56.17, H, 3.43, N, 2.98; found: C 56.40, H 3.30, N 2.71.

Diethyl {2-[3,7-di(thiophen-3-yl)-10H-phenothiazin-10-yl]ethyl}phosphonate (4)



Diethyl {2-[3,7-di(thiophen-3-yl)-10H-phenothiazin-10-yl]ethyl}phosphonate (**3**, 1.2 g, 2.55 mmol) was suspended in triethyl phosphite (3 ml, 51 mmol) and the reaction was refluxed overnight. After termination of reaction (TLC, eluent acetone:*n*-hexane, 7:18), solvent was removed under reduced pressure and the crude product was purified by column chromatography (eluent acetone:*n*-hexane, 7:18). Product obtained as yellow resin (1.05 g, 78 %). ¹H NMR (400 MHz, DMSO-*d*₆): δ 7.83 (s, 2H), 7.63 – 7.52 (m, 8H), 7.05 (d, *J* = 8.4 Hz, 2H), 4.15 – 3.94 (m, 6H), 2.35 – 2.20 (m, 2H), 1.24 (t, *J* = 7.1 Hz, 6H) ppm. ¹³C NMR (101 MHz, DMSO-*d*₆): δ 142.43, 140.16, 130.00, 126.99, 125.96, 125.41, 124.51, 123.37, 120.04, 115.49, 61.35, 61.29, 40.93, 23.79, 22.45, 16.31, 16.26 ppm. Anal. calcd. for C₂₆H₂₆NO₃PS₃: C 59.18, H, 4.97, N, 2.65; found: C 59.41, H 4.89, N 2.88.

{2-[3,7-Di(thiophen-3-yl)-10H-phenothiazin-10-yl]ethyl}phosphonic acid (Th-2EPT or V1495 SAM)



Diethyl {2-[3,7-di(thiophen-3-yl)-10*H*-phenothiazin-10-yl]ethyl}phosphonate (**4**, 1 g, 1.89 mmol) was dissolved in anhydrous 1,4-dioxane (25 ml) under argon atmosphere. Afterwards, bromotrimethylsilane (2.5 ml, 18.9 mmol) was added dropwise and reaction was stirred overnight at 25 °C. After consumption of phosphonate **5** (TLC, eluent acetone:*n*-hexane, 8:17) methanol (0.8 ml, 18.9 mmol) was added and stirring continued for 2 hours. Afterwards, distilled water was added dropwise until precipitate was formed and stirring continued overnight. Product was purified by dissolving in minimum amount of THF, precipitating into 20-fold excess of *n*-hexane, filtering, and washing with *n*-hexane to give brown crystals (0.62 g, 70 % yield). M.p. 198–200 °C (melting and decomposition). ¹H NMR (400 MHz, DMSO-*d*₆): δ 7.80 (s, 2H), 7.62 – 7.57 (m, 2H), 7.58 – 7.47 (m, 6H), 7.01 (d, *J* = 8.4 Hz, 2H), 4.13 – 3.98 (m, 2H), 2.16 – 2.00 (m, 2H) ppm. ¹³C NMR (101 MHz, DMSO-*d*₆): δ 142.33, 140.16, 129.89, 126.98, 125.96, 125.42, 124.45, 122.75, 119.98, 115.17, 41.98, 26.33, 25.03 ppm. Anal. calcd. for C₂₂H₁₈NO₃PS₃: C 56.04, H, 3.85, N, 2.97; found: C 56.20, H 4.01, N 2.83.

NMR spectra of synthesized compounds

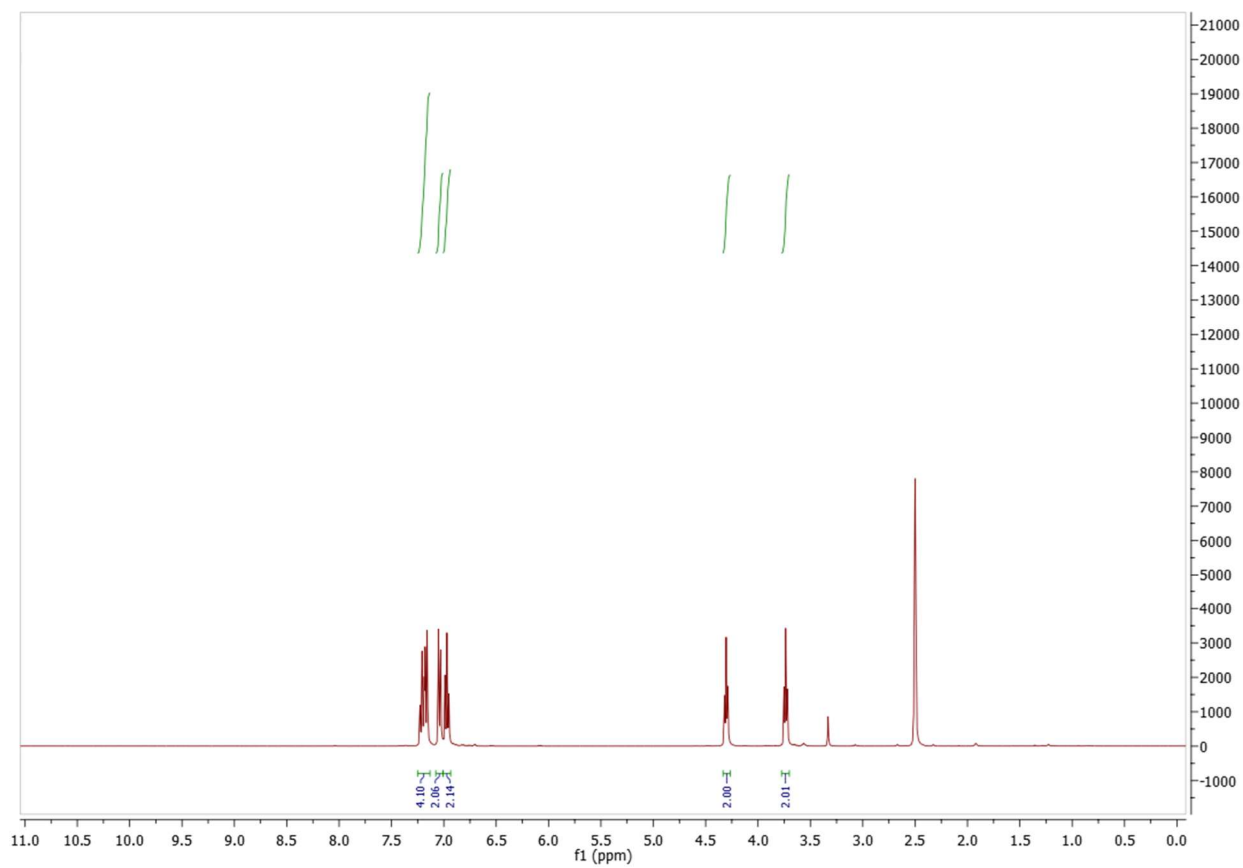
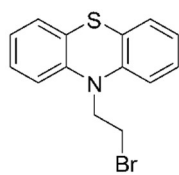


Figure S11 ^1H NMR spectrum of compound 1 in DMSO- d_6

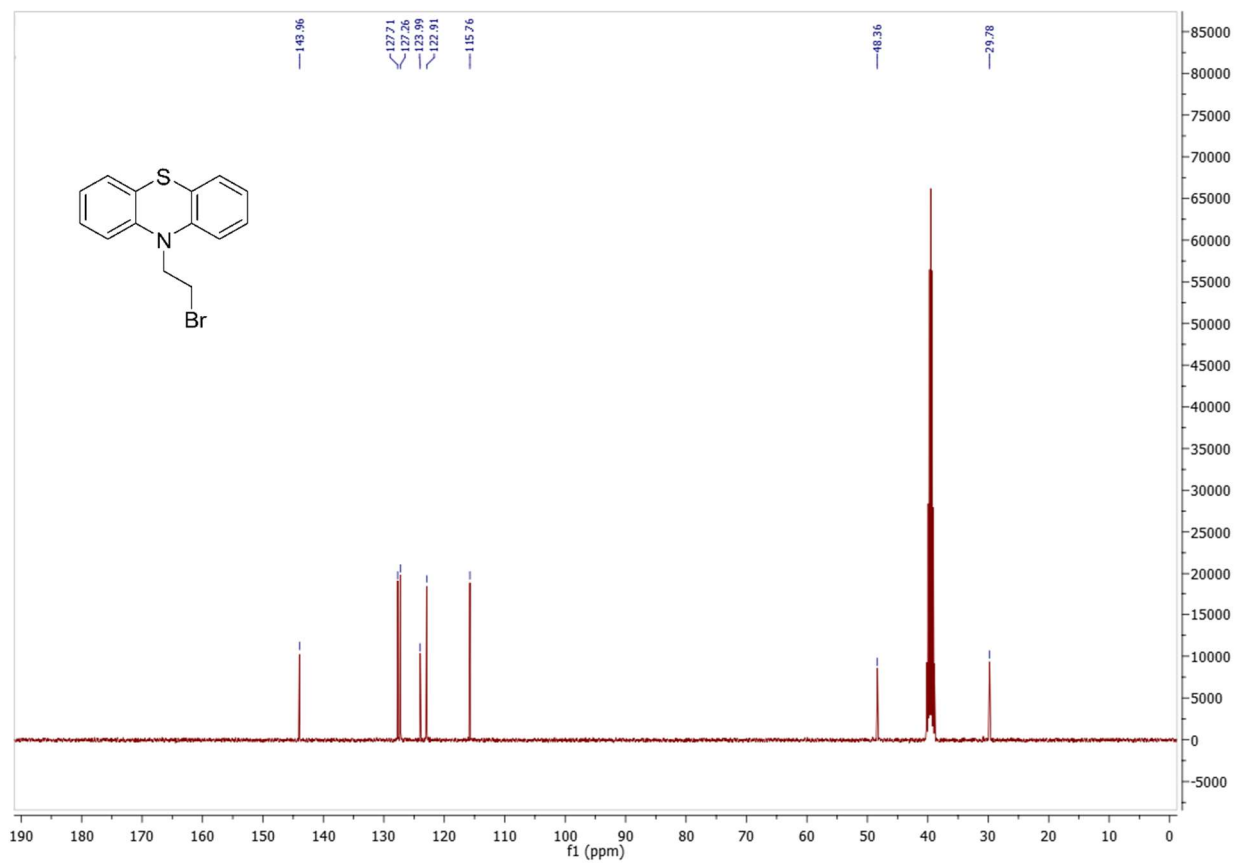


Figure S12 2 ^{13}C NMR spectrum of compound 1 in DMSO- d_6

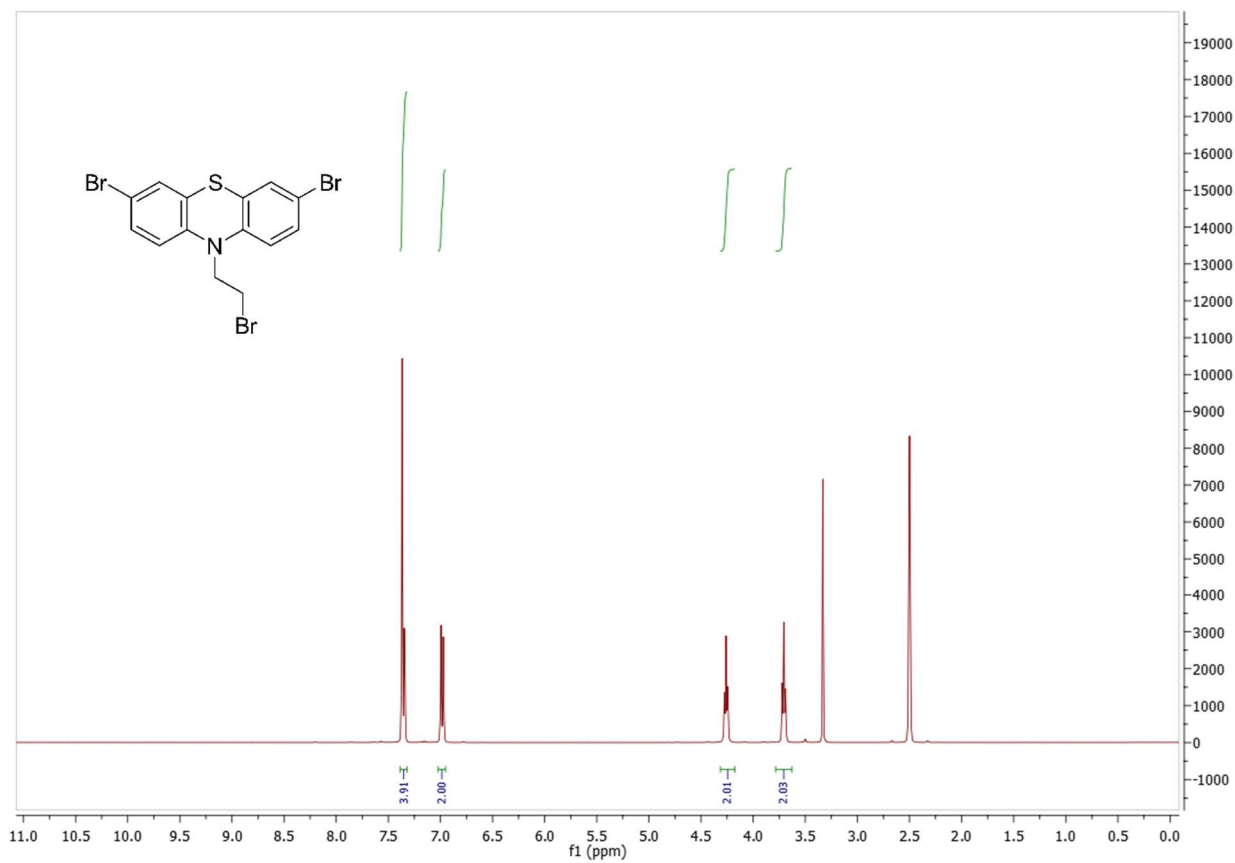


Figure S133 ^1H NMR spectrum of compound 2 in DMSO- d_6

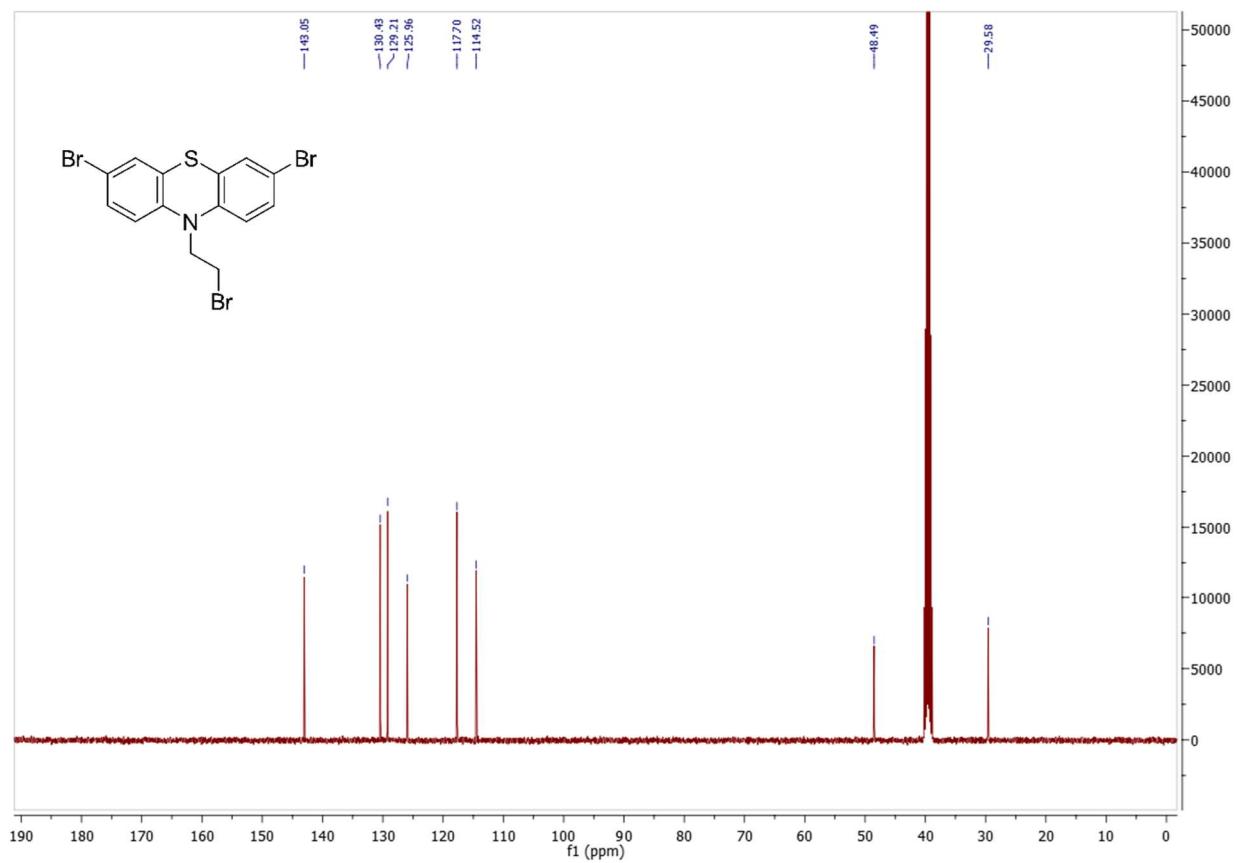


Figure S144 ^{13}C NMR spectrum of compound 2 in DMSO-d_6

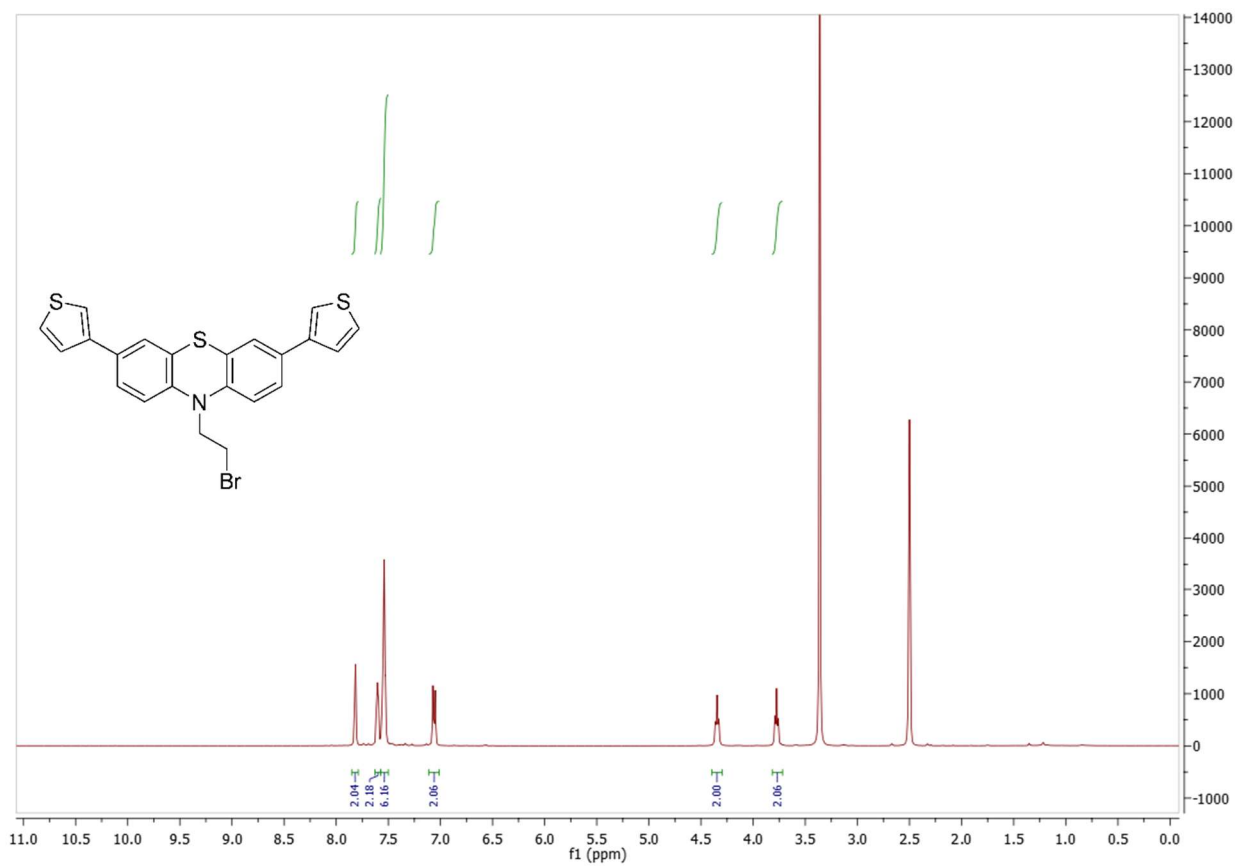


Figure S155 ^1H NMR spectrum of compound **3** in DMSO-d_6

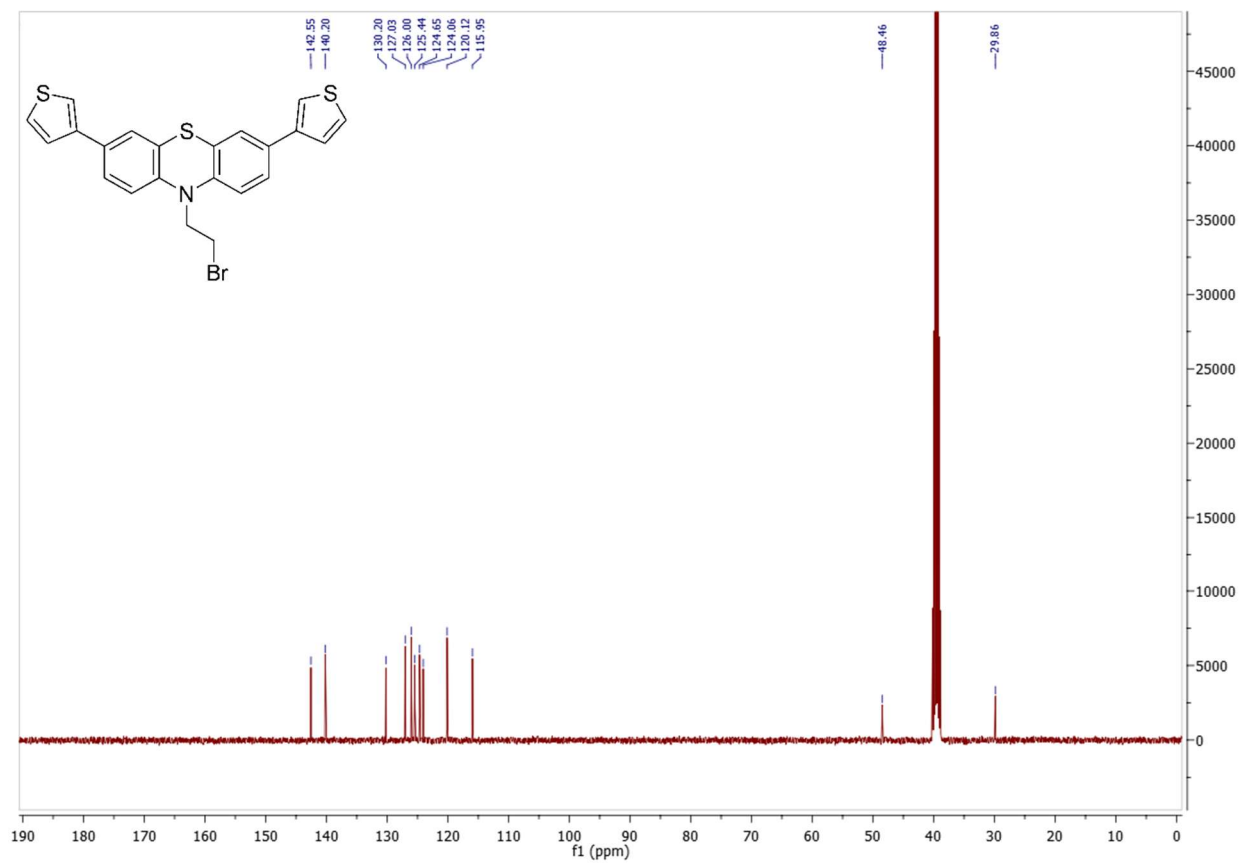


Figure S166 ^{13}C NMR spectrum of compound **3** in DMSO-d_6

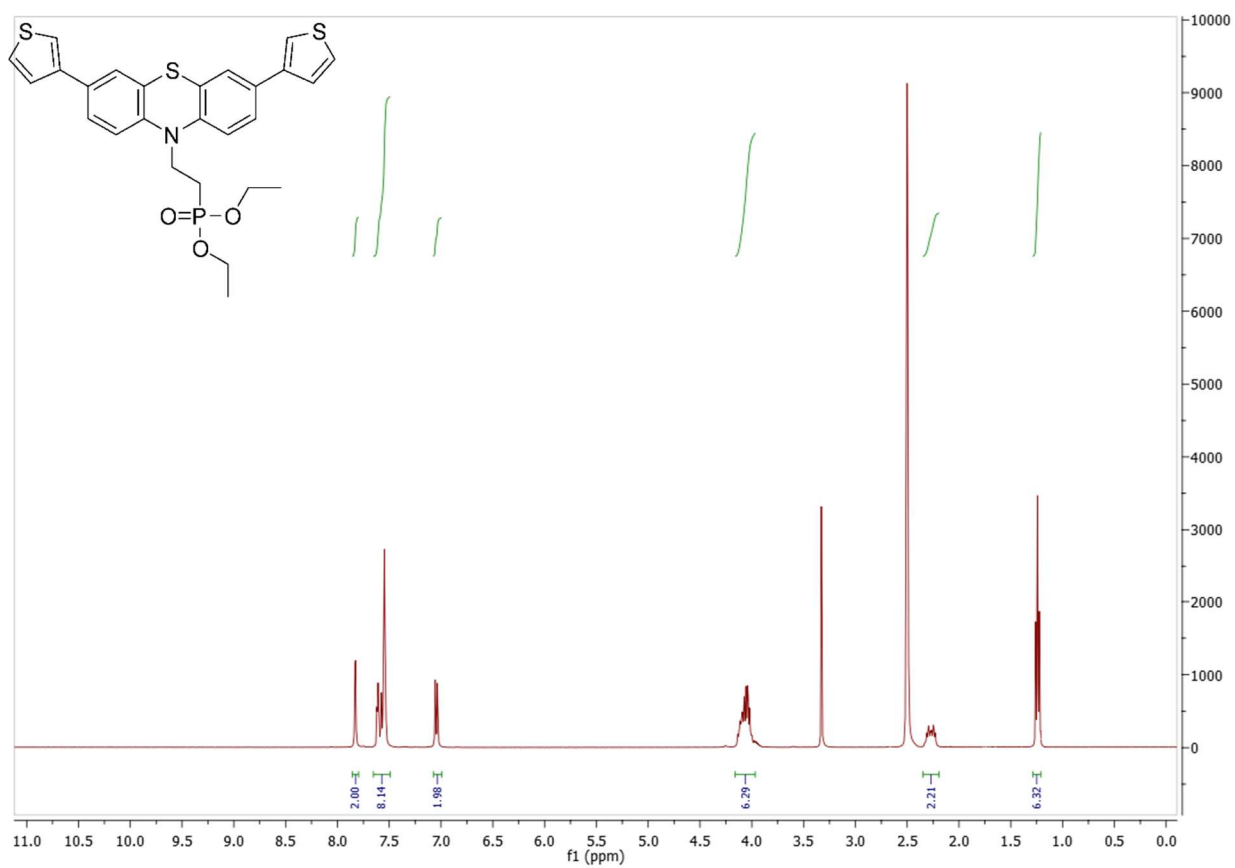


Figure S177 ¹H NMR spectrum of compound 4 in DMSO-d₆

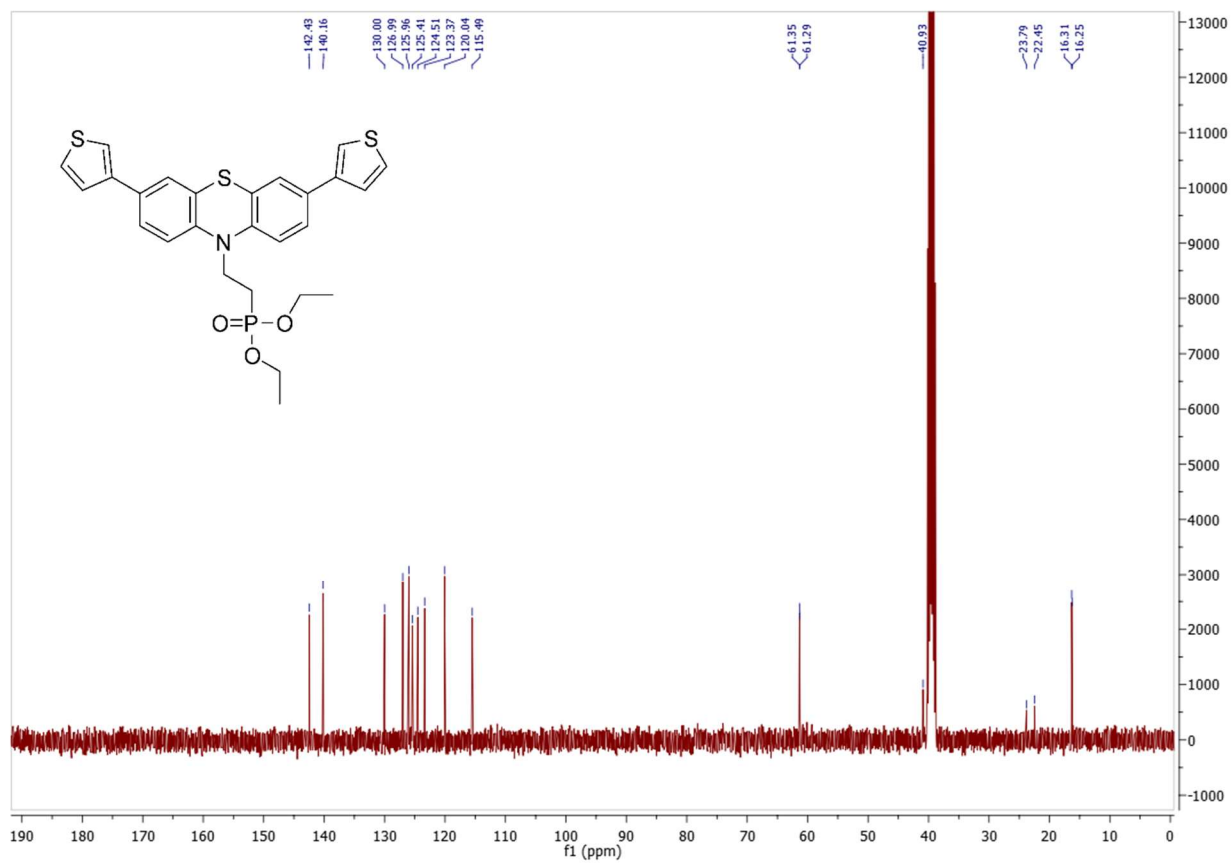


Figure S188 ^{13}C NMR spectrum of compound **4** in DMSO-d_6

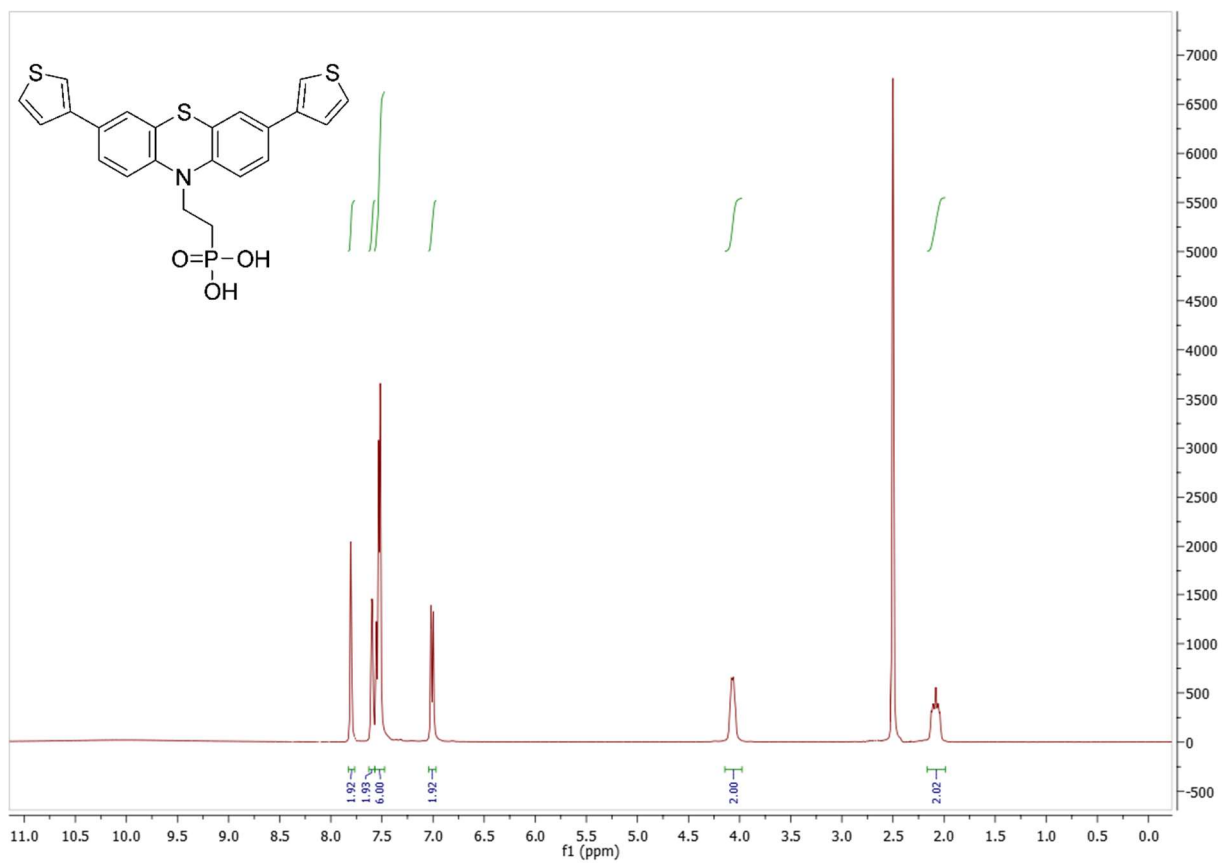


Figure S199 ^1H NMR spectrum of Th-2EPT in DMSO-d_6

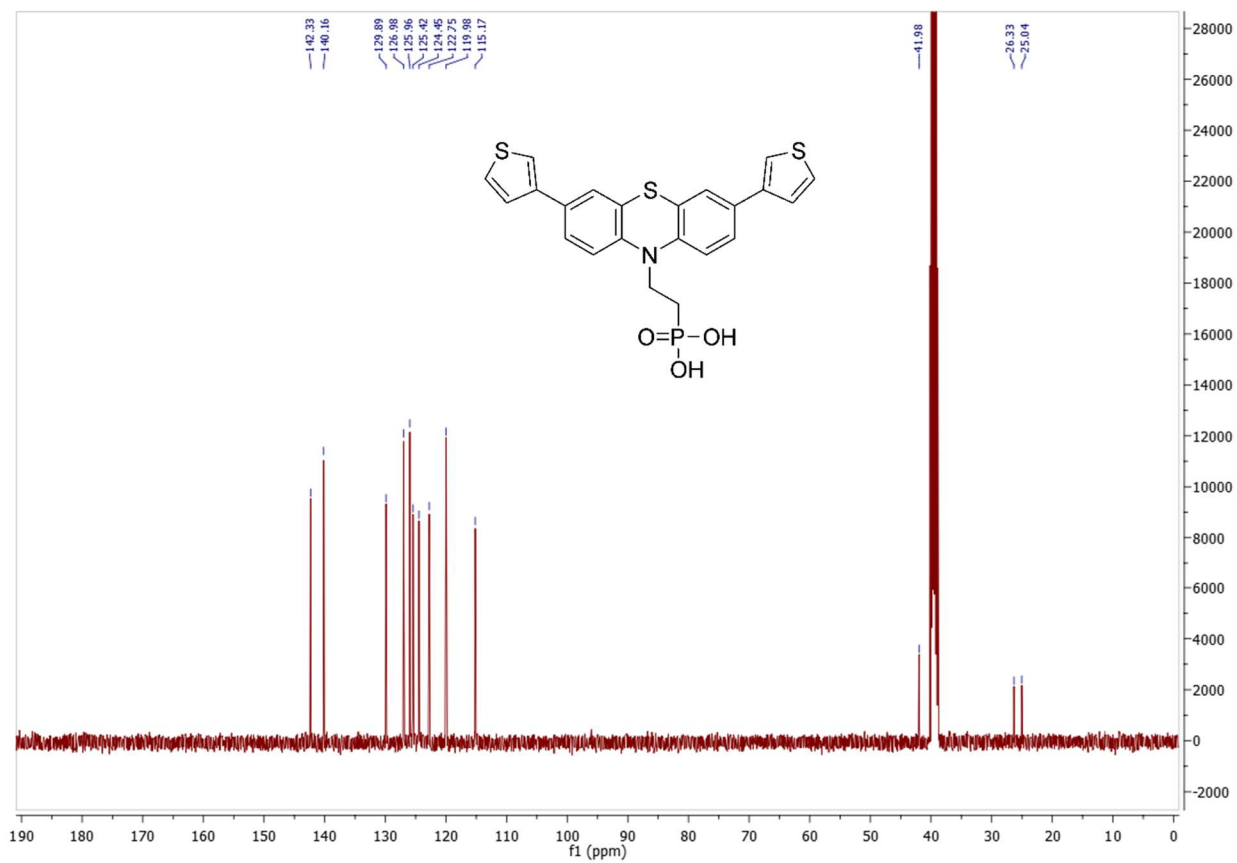


Figure S210 ^{13}C NMR spectrum of Th-2EPT in DMSO-d_6

Photoelectrical measurements

The solid-state ionization potential (I_p) of the layer of the synthesized Th-2EPT SAM was measured by the electron photoemission in the air method. The sample for the ionization energy measurement was prepared by dissolving material in THF, and the solutions was coated on Al plates that were pre-coated with a $\sim 0.5 \mu\text{m}$ thick methylmethacrylate and methacrylic acid copolymer adhesive layer. The thickness of the transporting material layer was $0.5\text{--}1 \mu\text{m}$. The samples were illuminated with monochromatic light from the quartz monochromator with a deuterium lamp. The power of the incident light beam was $(2\text{--}5)\cdot 10^{-8} \text{ W}$. The negative voltage of -300 V was supplied to the sample substrate. The counter electrode with the $4.5\times 15 \text{ mm}^2$ slit for illumination was placed at an 8 mm distance from the sample surface. The counter-electrode was connected to the input of the BK2-16 type electrometer working in the open input regime for the photocurrent measurement. The $10\text{--}15 \text{--}10\text{--}12 \text{ A}$ strong photocurrent was flowing in the circuit under illumination. Photocurrent I is strongly dependent on the incident light photon energy $h\nu$. The $I^{0.5} = f(h\nu)$ dependence chart was plotted. The linear part of this dependence was extrapolated to the $h\nu$ axis, and the I_p value was determined as the photon energy at the interception point.

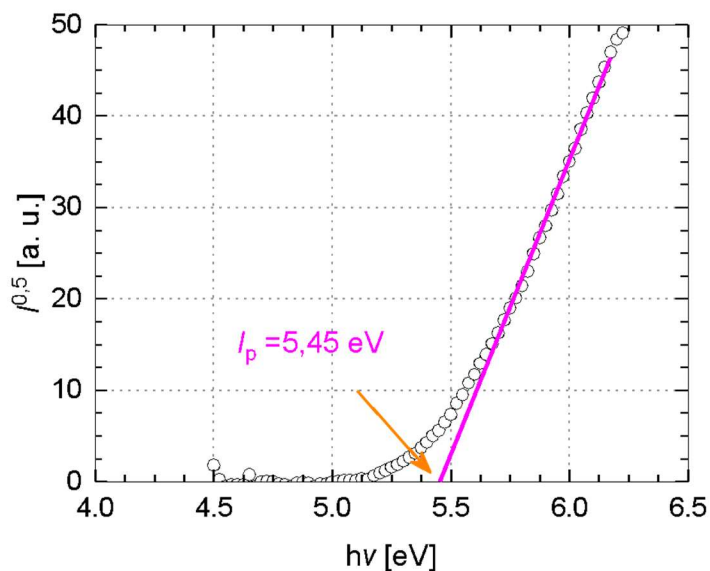


Figure S2111 I_p measurement on Th-2EPT

References

1. Blum, V. *et al.* Ab initio molecular simulations with numeric atom-centered orbitals. *Comput. Phys. Commun.* **180**, 2175–2196 (2009).
2. Stephens, P. J., Devlin, F. J., Chabalowski, C. F. & Frisch, M. J. Ab Initio Calculation of Vibrational Absorption and Circular Dichroism Spectra Using Density Functional Force Fields. *J. Phys. Chem.* **98**, 11623–11627 (1994).
3. Simon, S., Duran, M. & Dannenberg, J. J. Effect of Basis Set Superposition Error on the Water Dimer Surface Calculated at Hartree–Fock, Møller–Plesset, and Density Functional Theory Levels. *J. Phys. Chem. A* **103**, 1640–1643 (1999).
4. Lange, I. *et al.* Tuning the Work Function of Polar Zinc Oxide Surfaces using Modified Phosphonic Acid Self-Assembled Monolayers. *Adv. Funct. Mater.* **24**, 7014–7024 (2014).
5. Liu, X., Wang, L. & Tong, Y. Optoelectronic Properties of Ultrathin Indium Tin Oxide Films: A First-Principle Study. *Crystals* **11**, 30 (2020).
6. Ricciarelli, D., Meggiolaro, D., Ambrosio, F. & De Angelis, F. Instability of Tin Iodide Perovskites: Bulk p-Doping versus Surface Tin Oxidation. *ACS Energy Lett.* **5**, 2787–2795 (2020).